A Combined Eddy-Diffusivity Mass-Flux Approach for the Convective Boundary Layer

A. PIER SIEBESMA

Royal Netherlands Meteorological Institute (KNMI), De Bilt, Netherlands

PEDRO M. M. SOARES

University of Lisbon, CGUL, IDL, and Department of Civil Engineering, Instituto Superior de Engenharia de Lisboa, Lisbon, Portugal

JOÃO TEIXEIRA

NATO Undersea Research Centre, La Spezia, Italy

(Manuscript received 29 July 2005, in final form 1 July 2006)

ABSTRACT

A better conceptual understanding and more realistic parameterizations of convective boundary layers in climate and weather prediction models have been major challenges in meteorological research. In particular, parameterizations of the dry convective boundary layer, in spite of the absence of water phase-changes and its consequent simplicity as compared to moist convection, typically suffer from problems in attempting to represent realistically the boundary layer growth and what is often referred to as countergradient fluxes. The eddy-diffusivity (ED) approach has been relatively successful in representing some characteristics of neutral boundary layers and surface layers in general. The mass-flux (MF) approach, on the other hand, has been used for the parameterization of shallow and deep moist convection. In this paper, a new approach that relies on a combination of the ED and MF parameterizations (EDMF) is proposed for the dry convective boundary layer. It is shown that the EDMF approach follows naturally from a decomposition of the turbulent fluxes into 1) a part that includes strong organized updrafts, and 2) a remaining turbulent field. At the basis of the EDMF approach is the concept that nonlocal subgrid transport due to the strong updrafts is taken into account by the MF approach, while the remaining transport is taken into account by an ED closure. Large-eddy simulation (LES) results of the dry convective boundary layer are used to support the theoretical framework of this new approach and to determine the parameters of the EDMF model. The performance of the new formulation is evaluated against LES results, and it is shown that the EDMF closure is able to reproduce the main properties of dry convective boundary layers in a realistic manner. Furthermore, it will be shown that this approach has strong advantages over the more traditional countergradient approach, especially in the entrainment layer. As a result, this EDMF approach opens the way to parameterize the clear and cumulus-topped boundary layer in a simple and unified way.

1. Introduction

The traditional way to parameterize turbulent transport in the atmospheric boundary layer is through an eddy-diffusivity approach. This method estimates the vertical turbulent flux $\overline{w'\phi'}$ of a field ϕ as the product of the local gradient of the mean value of ϕ and an eddy-diffusivity coefficient K. One well-known drawback of this method is that it cannot adequately describe an upward turbulent heat flux in the upper part of the convective boundary layer, where often a slightly stable potential temperature profile is observed. In order to resolve this deficiency, the so-called countergradient term has been introduced (Ertel 1942), which takes into account the capability of rising plumes to ascent counter to the mean gradient.

The most popular format that takes this effect into account is the one proposed by Deardorff (1966), which, when applied to the potential temperature θ, can be written as

Corresponding author address: A. Pier Siebesma, Royal Netherlands Meteorological Institute (KNMI), P.O. Box 201, 3730 AE De Bilt, Netherlands.
E-mail: siebesma@knmi.nl

DOI: 10.1175/JAS3888.1

$$\overline{w'\theta'} = -K\frac{\partial\overline{\theta}}{\partial z} + \overline{w'\theta'_{\rm NL}}; \quad \overline{w'\theta'_{\rm NL}} = K\gamma, \tag{1}$$

where all notation is conventional: w denotes the vertical velocity, overbars indicate a spatial average, primes deviations from these averages, and γ quantifies the effect of the nonlocal transport. This formulation has been subject of numerous attempts to formally justify the nonlocal term γ on the basis of second-order equations (Deardorff 1972; Holtslag and Moeng 1991) and interesting analytical quasi-steady solutions of this form have been reported recently (Stevens 2000). All these studies have concentrated exclusively on how the nonlocal format (1) can faithfully reproduce the internal structure of the convective boundary layer, although occasional claims have been made on how (1) might influence the interaction between the boundary layer and the free atmosphere (Holtslag et al. 1995; Stevens 2000).

Our main objective is to introduce a novel way to take into account the effect of strong thermals in the convective boundary layer for use in climate and numerical weather prediction (NWP) models. Contrary to the previous mentioned studies, our emphasis will be on developing a formulation that is also capable of realistically ventilating heat and moisture into the free atmosphere and, in the case of a cloudy boundary layer, into the cloud layer aloft. In fact, the original motivation of this study arose from the need to design a unified parameterization of turbulent transport in the cloud-topped boundary layer. State-of-the-art parameterizations suffer from the undesired situation that advective mass-flux parameterizations used for convective transport in the cumulus cloud layer are usually matched in an arbitrary and ad hoc manner with the eddy-diffusivity approach in the subcloud layer. In order to overcome this situation, we will propose a new method that combines the advective mass-flux approach and the eddy-diffusivity method in a coherent way, so that it paves the way for a unified parameterization of turbulent transport in the cloud-topped boundary layer. The whole concept is based on a separate treatment of the organized strong updrafts and the remaining turbulent field. The organized, strongly skewed, and nonlocal updrafts are described by an advective mass-flux approach, whereas the remaining turbulent part is represented by an eddy-diffusivity approach. The basic idea has been formulated in Siebesma and Teixeira (2000) and practical applications of this approach to the cloud-topped boundary layer have been discussed recently in Soares et al. (2004). The main purpose of this paper is to formulate a theoretical framework for this approach with the aid of LES results, to evaluate it and compare it with other standard approaches.

The set up of this study is as follows. In section 2 we introduce the basic concepts that will constitute our approach; in section 3 we present LES results of a number of dry convective boundary layer cases that will be used throughout this study. Section 4 will be dedicated to the various closures of the parameterization scheme using the LES results of section 2. In section 5, the scheme will be evaluated and compared with other approaches. Perspectives and conclusions are presented in section 6.

2. Problem formulation and basic concept of the eddy-diffusivity mass-flux approach

The time evolution of a field $\phi \in \{\theta, q_v\}$ in the Boussinesq approximation is described by

$$\frac{\partial\overline{\phi}}{\partial t} = -\frac{\partial\overline{w'\phi'}}{\partial z} + F_\phi, \tag{2}$$

where the first term on the right-hand side (rhs) describes the tendency due to turbulent mixing and convection and the remaining term F_ϕ contains all tendency terms due to advection and diabatic processes. In the absence of any diabatic processes and a zero mean wind, the total tendency is simply described by the turbulent flux divergence.

To parameterize the turbulent flux in the boundary layer, we start by designing a separation between strong organized updrafts and the remaining turbulence, such as is sketched schematically in Fig. 1. To be more specific, we define this strong updraft as a fixed fractional area a_u, say a few percent of the horizontal domain under consideration, that contains the strongest upward vertical velocities. We will make this notion more precise later in the paper. Subsequently, we can decompose the total turbulent flux of any arbitrary variable ϕ without any approximation into three terms (Siebesma and Cuijpers 1995)

$$\overline{w'\phi'} = a_u\overline{w'\phi'}^u + (1-a_u)\overline{w'\phi'}^e + a_u(w_u - \overline{w})(\phi_u - \phi_e), \tag{3}$$

where the sub- and superscripts u and e refer to the strong updrafts and the complementary environmental part. The third term of the rhs of (3) is usually referred to as the mass-flux contribution where a convective mass flux can be defined as $M \equiv a_u(w_u - \overline{w})$. If we now make use of the fact that $a_u \ll 1$ we can neglect the first term on the rhs of (3) and approximate $\phi_e \simeq \overline{\phi}$, so that (3) can be simplified to

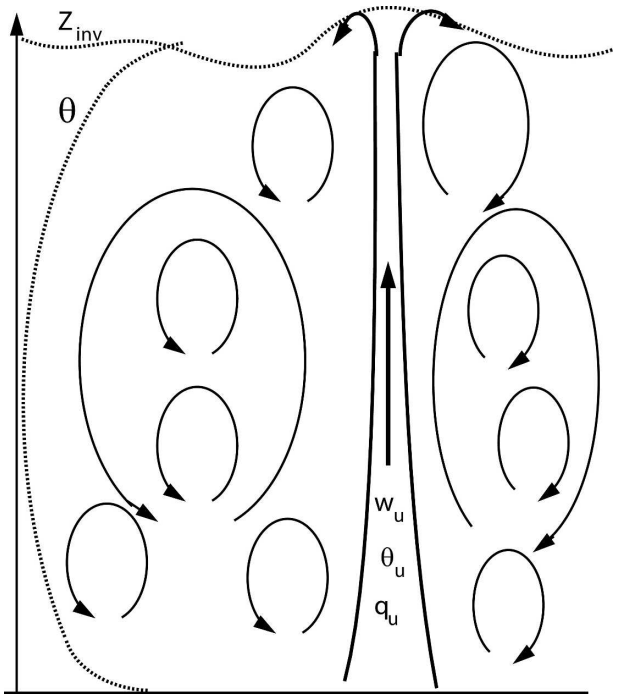

FIG. 1. Sketch of a convective updraft embedded in a turbulent eddy structure.

$$\overline{w'\phi'} \simeq \overline{w'\phi'^e} + M(\phi_u - \overline{\phi}). \tag{4}$$

As we have now isolated the nonlocal transport through the mass-flux term we make the final step in approximating the remaining turbulent transport term by an eddy-diffusivity approach:

$$\overline{w'\phi'} \simeq -K\frac{\partial\overline{\phi}}{\partial z} + M(\phi_u - \overline{\phi}). \tag{5}$$

All that is needed to put this eddy-diffusivity mass-flux (EDMF) approach into gear is to obtain coefficients for the eddy diffusivity, the mass flux, and a model for the updraft fields. This will be the topic of section 4.

Before we proceed further with the practical implementation of this model, let us pause for a moment to discuss the realism and motivation of the proposed two scale separation in some more detail. Historically, the mass-flux concept originates from the cloud modeling community (Arakawa 1969; Yanai et al. 1973; Ogura and Cho 1973; Betts 1973). This is not surprising when realizing that the joint probability density function (PDF) of w and any moist conserved variable ϕ in the cloud layer has a well-defined bimodal structure: one peak that is associated with the strong updrafts in the cloudy cores and a second maximum that is associated with the cloud induced subsidence. This bimodal structure of the PDF, obviously the result of condensational processes in the cloud layer, is exactly the reason that the mass-flux concept works so well in the cloud layer. That is to say that the second term of the rhs of (5) is a good approximation of the turbulent flux in the cloud layer. As a result, virtually all present moist convection parameterizations utilize relation (5) and, moreover, simply ignore the first term of the rhs of (5).

For the dry convective boundary layer, the situation is rather different: the joint PDF of w and θ only has one maximum near $(\overline{\theta}, \overline{w})$ (Wyngaard and Moeng 1992). Therefore, virtually all attempts to model turbulent transport in the convective boundary layer with a mass-flux approach utilize a decomposition in updrafts $(w > \overline{w})$ and downdrafts $(w < \overline{w})$ (Chatfield and Brost 1987; Randall et al. 1992; Lappen and Randall 2001a; Petersen et al. 1999; Wang and Albrecht 1990). One of the reasons for this choice is probably that, for the dry convective boundary layer, there is no other decomposition for which the mass flux term in (5) gives a larger contribution to the total flux.

In this study, we utilize a decomposition between strong thermals and the remaining complementary part and build an EDMF model on this. The motivation for this approach is twofold. First, the dynamics of a thermal is strongly nonlocal since its kinetic energy in the upper part of the boundary layer is largely due to the buoyancy production in the lower half of the boundary layer. It is for this reason that an eddy-diffusivity approach based on the local gradient of the mean field is inappropriate for this important transport mechanism. A mass-flux concept is well capable of taking into account these nonlocal effects and hence we will apply this concept to these thermals. Second, thermals ultimately can be considered as the invisible roots of the clouds that feed on them (Lemone and Pennell 1976). Therefore, a mass-flux description of these thermals allows for a natural extension of the dry convective boundary layer to the cloudy cores in the cloud layer. As these cloudy cores cover typically an area of only a few percent it is clear that an updraft–downdraft decomposition in which updrafts have a fraction of around 40% in the subcloud layer does not provide a continuous description between the subcloud and cloud layer.

That leaves us with the question how to come up with a simple operational definition of thermals (Haij 2005; Krusche and Oliveira 2004; Lenschow and Stephens 1980). As they are coherent spatial structures, they do not show up in a Fourier power spectrum of w, θ, or q_v (but neither do cloud structures). However, they can be well identified as a peak in the global wavelet spectrum (Haij 2005; Krusche and Oliveira 2004). This peak defines the typical thermal size of 50 $\sim$ 100 m near the

TABLE 1. Definition of the setup of the cases.

Case	Lapse rate γ K km^{-1}	Surface flux Q_* K m s^{-1}
01	1.95	0.06
02	2.93	0.06
03	3.90	0.06
04	1.95	0.03
05	2.93	0.03
06	3.90	0.03

surface and which is increasing with height. Using this length scale as a criterion, during which positive anomalies in observed w fields have to persist, results in a fractional area cover of the thermals between 1% and 4% (Haij 2005). These percentages coincide well with the area fraction of buoyant updrafts in the cloudy cores in the case of a cloud-topped boundary layer (Siebesma and Cuijpers 1995; Stevens et al. 2001; Brown et al. 2002; Siebesma et al. 2003). Observations also show that the highest vertical velocities are predominantly present within these thermal structures.

On the basis of these findings we define strong updrafts at a given height z in the LES model as all the grid points with a positive vertical velocity larger than the p percentile of the w distribution at that height (van Ulden and Siebesma 1997). This p-percentile velocity $w_{p\%}(z)$ is defined as the vertical velocity for which exactly a percentage p of the distribution contains grid points with a vertical velocity larger than $w_{p\%}(z)$ at height z. Thus the strong updraft ensemble at a height z is simply defined as all the grid points that obey the condition $w(x, y, z) > w_{p\%}(z)$. Since we use values for p of the order of 1% to 5% (see section 3), this definition is in line with observations of thermals analyzed with wavelets (Haij 2005), and it provides an appropriate matching with the cloudy cores that feed on these thermals. We anticipate that the mass-flux contribution for the convective boundary layer with this decomposition will not be so dominant in (5) as in the case for cloudy cores in the cloud layer. It is exactly for this reason that we will not ignore the first term of the rhs of (5) in the present model.

Finally, note that (5) has the same format as the original countergradient formulation (1). In the present formulation, however, the nonlocal flux is described explicitly by a mass-flux term.

3. LES experiments

The LES code used here is the one described in Cuijpers and Duynkerke (1993) and Siebesma and Cuijpers (1995). The basic equation sets are formulated within the Boussinesq formulation. The advection terms are numerically solved using a second order centered difference scheme and for the subgrid-scale turbulence a 1½-order closure scheme is employed for which an additional prognostic equation for the subgrid turbulent kinetic energy (TKE) is solved. The simulations are performed on a numerical domain of $100 \times 100 \times 150$ grid points using a uniform grid spacing of $\Delta x = \Delta y = 50$ m and $\Delta z = 20$ m. In this study only dry free convective flows are considered. A series of six LES runs were carried out with different heat surface fluxes $\overline{w'\theta'_s} = Q_*$ and different initial lapse rates $(\partial\theta/\partial z) \equiv \gamma$ (see Table 1). All runs start with the same surface potential temperature of 297.2 K and surface pressure that is set to a value of 1000 mb. The mean horizontal wind is set to zero in these simulations. Case 1 (see Table 1) is related to a previous intercomparison case of LES codes for the dry convective boundary layer (Nieuwstadt et al. 1991).

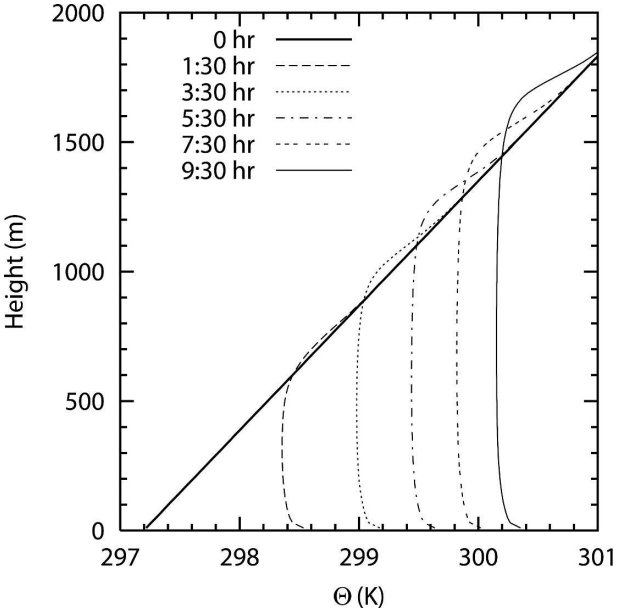

FIG. 2. Horizontally spatially averaged profiles of the LES output of θ for case 1 at initialization time and at t = 1:30, 3:30, 5:30, 7:30, 9:30 h after the initialization time.

As an example, the mean profiles of potential temperature of case 1 are shown in Fig. 2 with time intervals of 2 h along with the initial profile. Besides the obvious deepening of the convective boundary layer, one can also observe an increasing inversion strength as a function of time which is due to the top entrainment process. In order to show simultaneous LES results for different cases and at different stages of the simulation it is convenient to nondimensionalize the results by introducing an inversion height z_*, a convective velocity scale $w_* = (g\beta Q_* z_*)^{1/3}$ (where $\beta = 1/300$ K^{-1} is the

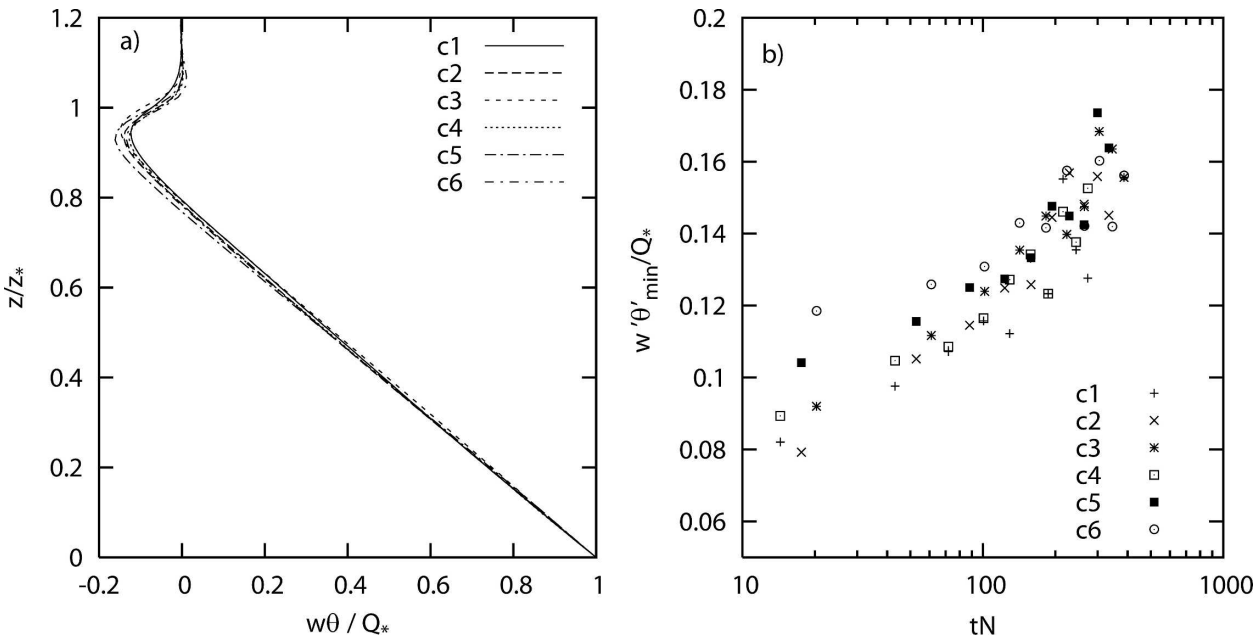

FIG. 3. (left) Dimensionless turbulent heat flux profiles $\overline{w'\theta'}/Q_*$ as a function of the dimensionless height z/z_* for the 10th hour for all six cases. (right) Hourly averaged dimensionless minimum heat flux values as a function of $\hat{t}$.

coefficient of thermal expansion), an eddy turnover time $t_* \equiv z_*/w_*$, and a temperature scale $\theta_* \equiv Q_*/w_*$. As an operational definition of the inversion height z_* we use the gradient method (Sullivan et al. 1998). In this method, for any location (x, y), the local inversion height is determined as the height where θ exhibits the maximum gradient. The (mean) inversion height z_* is then simply a spatial average over all the local inversion heights of the domain. This defines an inversion height that is slightly higher than the more conventional definition of z_* as the height where the buoyancy flux is a minimum (see Fig. 3a). The difference between these definitions is of the order of 5% to 10% which implies a difference of only 1% to 3 % for w_* and θ_*. One advantage of this definition is that it gives a smooth and continuous development of the boundary layer height with time (Sullivan et al. 1998).

Figure 3a shows the dimensionless heat fluxes $\overline{w'\theta'}/Q_*$ as a function of the normalized height z/z_* averaged over the ninth hour of the simulation for all cases. Note that the main difference for the dimensionless fluxes between the different cases is in the entrainment flux (i.e. the minimum value of the heat flux). Figure 3b zooms in further on this difference by showing the dimensionless entrainment flux for all cases at all hours as a function of dimensionless time $\hat{t} = tN$ where N is the Brunt–Väisälä frequency. The dimensionless entrainment flux increases with time to values around $0.17 \sim 0.2$ in agreement with previous studies of the entrainment zone (Fedorovich et al. 2004; Sullivan et al. 1998). The increase of the dimensionless entrainment flux is directly related with the sharpening of the inversion layer with time, as measured by the Richardson number $\mathrm{Ri} = \Delta\theta/\theta_*$ where $\Delta\theta$ is the temperature jump at the inversion. The lower values of the dimensionless entrainment flux in the earlier stages of the runs are due a less pronounced inversion jump. For details on the entrainment processes in the inversion layer on the basis of first- and second-order jump models we refer to two excellent papers by Fedorovich et al. (2004) and Sullivan et al. (1998).

In order to characterize the boundary layer growth for all cases, we normalize $z_*(t)$ by the growth the boundary layer would have had in the absence of any top entrainment. This so-called encroachment growth $z_e(t)$ is easily calculated as (Stull 1988)

$$z_e(t) = \left(\frac{2Q_*}{\gamma}t\right)^{1/2}. \tag{6}$$

For all cases, z_*/z_e converges to values within the interval [1.2, 1.3] (see also Fig. 12). One of the major evaluation tests will be whether the EDMF model and other related models are able to reproduce values within this interval.

As discussed in the previous section we will use p percentiles of the w field to define the strong updrafts. In order to display all mean and updraft profiles in one

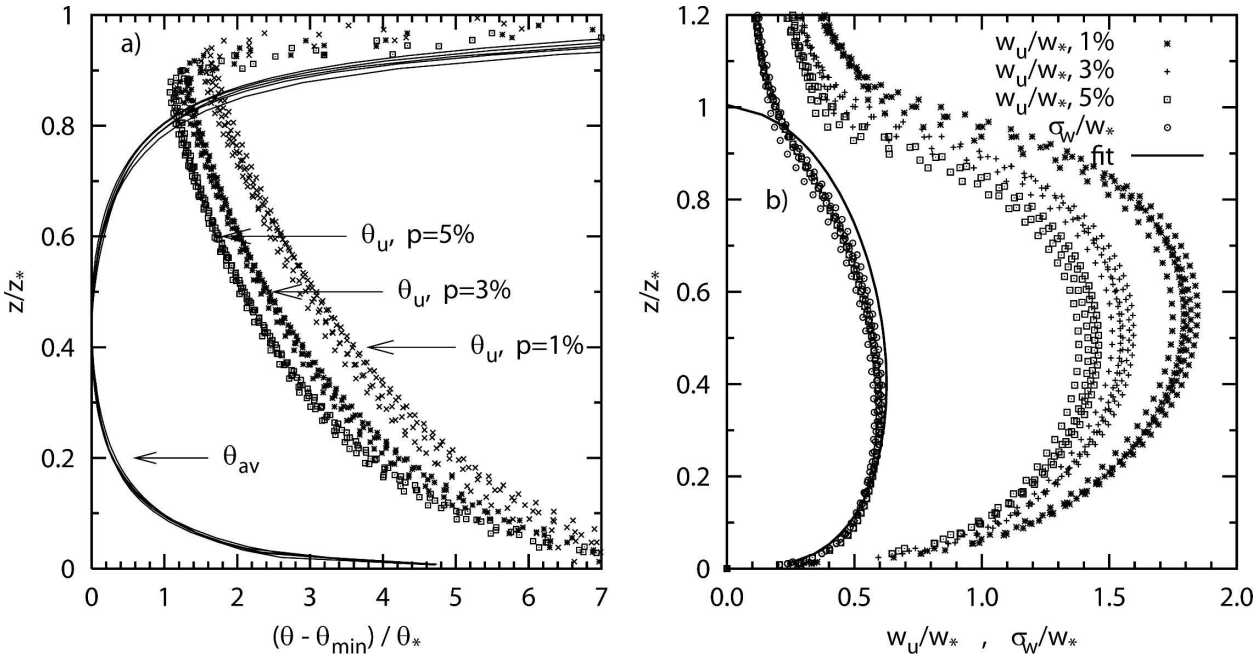

FIG. 4. (left) LES results of $(\overline{\theta} - \overline{\theta}_{\min})/\theta_*$ averaged over the sixth hour of the simulation along with updraft fields $(\theta_u - \overline{\theta}_{\min})/\theta_*$ for $p = 1\%, 3\%, 5\%$ for all cases. (right) LES results of the updraft vertical velocity for $p = 1\%, 3\%, 5\%$ along with an LES profile of σ_w rescaled with w_*. The line corresponds with the empirical expression (7).

plot we subtract the minimum value of the mean profile $\overline{\theta}_{\min}$ and rescale the result with θ_*. Figure 4 shows the results for $(\overline{\theta} - \overline{\theta}_{\min})/\theta_*$ and $(\theta_u - \overline{\theta}_{\min})/\theta_*$ for $p = 1\%$, 3%, 5% averaged over the sixth hour for all six cases. A number of observations can be made here that also apply to the other simulated hours. The average θ profile is characterized by a super-adiabatic part up to 0.4 z_* and a slightly stable part from 0.5 z_* upward. The updraft profile exhibits a positive temperature excess of $1 \sim 4$ times θ_* in most of the boundary layer but is changing sign as the updraft penetrates into the inversion around 0.8 z_*. Obviously, the excess temperature is larger as we increase our threshold values $w_{p\%}(z)$ through selecting smaller and more extreme updraft ensembles. Finally note that the updraft potential temperature is decreasing with height, which is a sign of lateral mixing of the updraft ensemble with the environment.

Figure 4b displays the dimensionless updraft velocities w_u/w_* along with the dimensionless standard deviation σ_w/w_* for $p = 1\%$, 3%, 5% again for all cases and averaged over the sixth hour. Also shown is an empirical expression for σ_w based on a combination of atmospheric data, tank measurements, and LES data (Holtslag and Moeng 1991)

$$\frac{\sigma_w}{w_*} \simeq 1.3\left[\left(\frac{u_*}{w_*}\right)^3 + 0.6\,\frac{z}{z_*}\right]^{1/3}\left(1 - \frac{z}{z_*}\right)^{1/2}, \quad (7)$$

where we use, in the absence of a mean horizontal wind, $u_* = 0$. The agreement in the boundary layer is good while the nonzero contributions for σ_w above the boundary layer is probably due to unphysical reflections that create waves that are not adequately damped by the sponge layer of the model. It can be observed that the updraft vertical velocity profiles scale well with σ_w with a proportionality factor $\mu = (\sigma_w/w_u)^2 \simeq 0.15$. This value is smaller than one would expect by assuming that the PDF of w is Gaussian. This is due to the fact the PDF of w is positively skewed (Wyngaard and Moeng 1992).

4. Eddy-diffusivity mass-flux parameterization for the convective boundary layer

In this section, we will use the LES results of the previous section to design a parameterization for turbulent heat transport in the convective boundary layer. Our starting point is (5). Therefore, our aim is to construct the simplest possible parameterization for the updraft fields $\phi \in \{\theta, q_v\}$; that is, to find an eddy-diffusivity K and a mass-flux M that are capable of realistically reproducing the time evolution of the boundary layer and the internal structure. We will also set up a parameterization for the updraft velocity w_u and use the height where this velocity approaches zero as a measure for the boundary layer height z_*.

a. The updraft model

The steady-state updraft budget equations for an arbitrary field ϕ within the mass-flux approximation are well known (Tiedtke et al. 1988; Siebesma and Holtslag 1996) and can be written as

$$\frac{1}{M}\frac{\partial M}{\partial z} = \epsilon - \delta \tag{8}$$

$$\frac{\partial M\phi_u}{\partial z} = \epsilon M\bar{\phi} - \delta M\phi_u + a_u F_{\phi_u}, \tag{9}$$

where ϵ and δ denote the fractional entrainment and detrainment rates, and F_{ϕ_u} contains all the external source and sink terms of the field ϕ in the updraft area a_u. For $\phi = \theta_u$ we set $F_{\phi_u} = 0$; that is, we assume no effects due to radiation and advection, so substitution of (8) in (9) gives a simple entraining updraft equation

$$\frac{\partial \theta_u}{\partial z} = -\epsilon(\theta_u - \bar{\theta}). \tag{10}$$

For the updraft velocity, the pressure and the buoyancy term are the two main source terms (Schumann and Moeng 1991)

$$F_{w_u} \simeq -\rho^{-1}\frac{\partial \bar{p}}{\partial z} + \beta g(\theta_{v,u} - \bar{\theta}_v)$$

$$\equiv P + B, \tag{11}$$

where the term $\bar{p}$ represents the part of the pressure that remains after subtracting the static pressure that obeys hydrostatic equilibrium. Within the spirit of the mass-flux approximation, we have neglected the pressure fluctuations within the updraft in (11). Substituting the forcing (11) in (9), using the definition of the mass-flux and rearranging terms gives the following steady-state budget equation for the vertical velocity

$$-\frac{1}{2}\frac{\partial w_u^2}{\partial z} - \epsilon_w w_u^2 + B + P = 0, \tag{12}$$

where the first term represents a transport term (T), the second term the entrainment term (E), and the last two terms represent the buoyancy and the pressure gradient term.

Note that we attached a w subscript to the fractional entrainment rate in (12) to indicate that the fractional entrainment rate of w can, in principle, be different from the entrainment rate of θ (de Roode and Bretherton 2003). The pressure term can conveniently be expressed in terms of the vertical velocity variance (Schumann and Moeng 1991)

$$P = -\frac{1}{\rho}\frac{\partial \bar{p}}{\partial z} = \frac{\partial \overline{w^2}}{\partial z} \simeq \frac{\partial \mu w_u^2}{\partial z}, \tag{13}$$

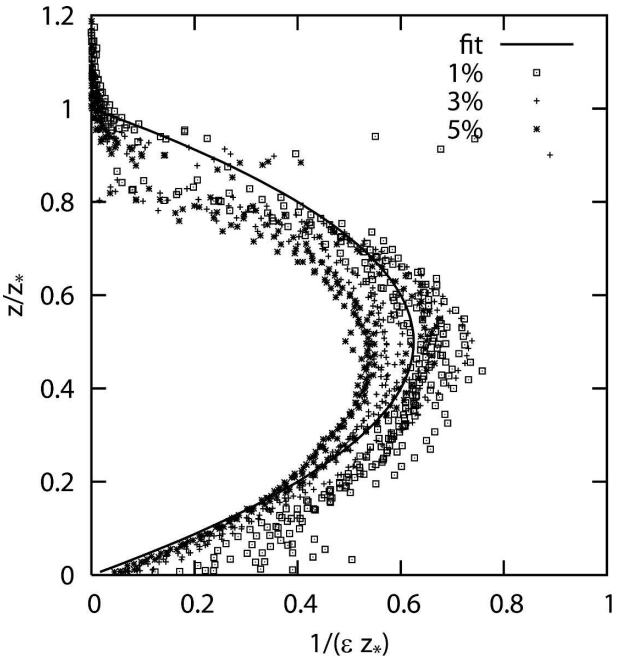

FIG. 5. LES results for the nondimensionalized reciprocal fractional entrainment rates $1/(\epsilon z_*)$ diagnosed using (10) for $p = 1\%$, 3%, 5% for all six cases averaged over the sixth hour. The full line represents the parameterized form (16).

where, in the last step, we have made use of the fact that w_u^2 scales well with the vertical velocity variance with a proportionality factor $\mu \simeq 0.15$ as discussed in the previous section. Finally, we assume that the fractional entrainment rate for the vertical velocity ϵ_w is proportional to the fractional entrainment rate for θ; that is,

$$\epsilon_w = b\epsilon. \tag{14}$$

Substituting (14) and (13) into the vertical updraft velocity equation (12) gives

$$\frac{1}{2}(1 - 2\mu)\frac{\partial w_u^2}{\partial z} = -b\epsilon w_u^2 + B. \tag{15}$$

Note that this vertical velocity equation has the same form as the one proposed by Simpson and Wiggert (1969) for cloudy plumes and which is widely used in moist convection parameterizations. The physical interpretation of the terms, however, is quite different.

The fractional entrainment rate ϵ is diagnosed using LES results for $\bar{\theta}$ and θ_u in (10). For the sixth hour we show in Fig. 5 the dimensionless fractional entrainment rate ϵz_* for $p = 1\%$, 3%, 5% for all cases. Although some systematic spread can be observed for these three definitions, the points collapse reasonably well on a single parabolic curve that can be well fitted with

$$\epsilon \simeq c_\epsilon\left(\frac{1}{z} + \frac{1}{z_* - z}\right) \tag{16}$$

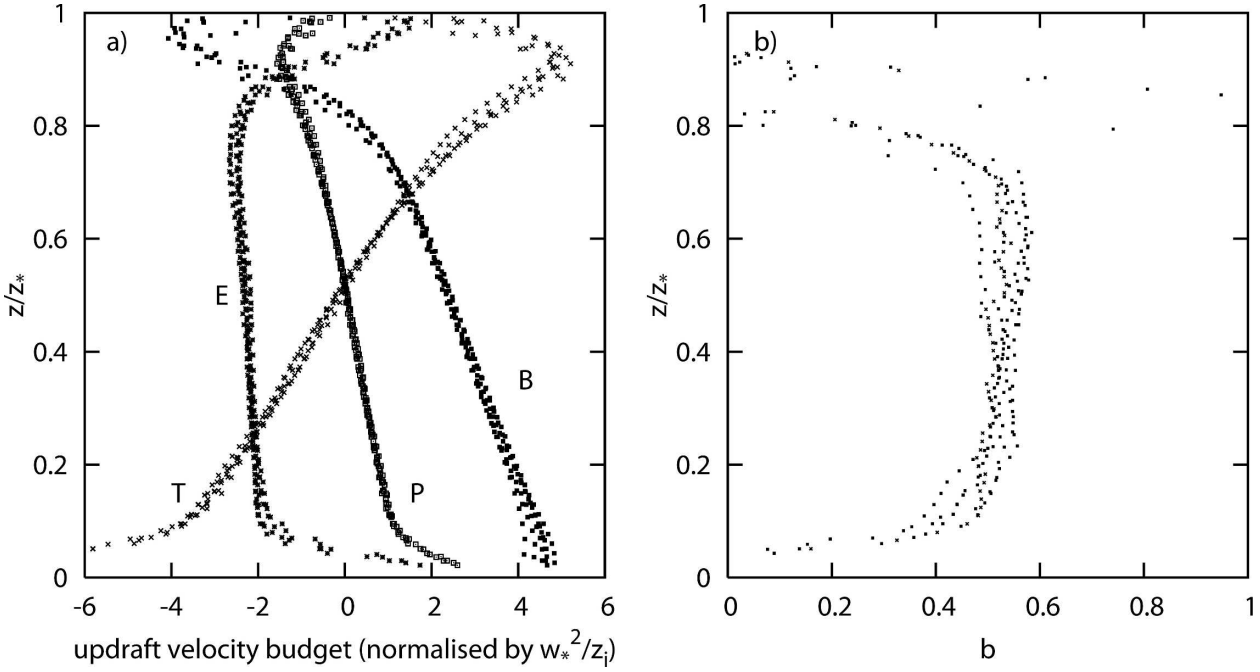

FIG. 6. (a) Nondimensionalized budget terms of the updraft velocity equation (12) as a function of the relative height for all cases averaged over the sixth hour, where T is the transport term, E is the entrainment term, B is the buoyancy term, and P is the pressure gradient term. (b) The corresponding diagnosed entrainment scaling parameter b [see (14)].

with $c_\epsilon \simeq 0.4$. This parabolic shape, already proposed in van Ulden and Siebesma (1997), strongly suggests that the entrainment length scale $\epsilon^{-1}(z)$ is determined by the dominant eddy size at height z (see also Fig. 1). Such an identification also explains the strong resemblance between ϵ^{-1} and the length scale used in TKE schemes (Cuxart et al. 2000; Bougeault and Lacarrère 1989; Teixeira et al. 2004). The use of (10) to diagnose ϵ becomes ill defined when the excess has a zero crossing. This explains the scatter of the diagnosed value of ϵ in Fig. 5 around the inversion.

The $\epsilon \sim z^{-1}$ behavior near the surface has been reported recently also, based on LES results, for a simple updraft–downdraft decomposition (de Roode et al. 2000). The z^{-1} scaling has the advantage that the precise choice of the initialization height z_1 becomes irrelevant in the limit of a neutral boundary layer. More precisely, if $\overline{\theta}$ has a logarithmic profile, it is easy to show, using (10) that for $\epsilon \sim z^{-1}$ the excess $\theta_u - \overline{\theta}$ becomes height independent (see appendix A). For the present cases, which are in the free convective limit, $\overline{\theta}$ is described by a power law in the surface layer. In that case, there is still a small dependency of the temperature excess, but still much smaller than in the case of a nonentraining adiabatic ascending plume.

Next we will evaluate the vertical velocity budget equation (12) with the LES results in its parameterized form. For the pressure term we use the right-hand side of (13), for the mixing term we use (14) along with the fit (16) for ϵ. We finally close the budget equation (12) of w by solving for b at each height level that is the remaining undetermined parameter [see (14)]. The budget terms are nondimensionalized by w_*^2/z_* and shown in the left panel of Fig 6. This allows averages to be shown over the sixth hour of the budget equation for all six cases. It can be observed that the most important source term for the updraft vertical velocity is the buoyancy term. The entrainment term is a remarkable constant sink term while the pressure term is a source term in the lower half of the boundary layer and a sink term in the upper half. Overall the sum of the three budget terms (B, P, E) generate a net source term in the lower part of the boundary layer and a net sink term in the upper part. This is compensated by the transport term T, reflecting the fact that kinetic energy is transported from the lower half to the upper half of the boundary layer by the nonlocal strong thermals.

The diagnosed profile of the scaling factor b is displayed in Fig. 6b. The fact that the diagnosed value of b is rather independent of height and time is a justification for the assumption that ϵ_w can be scaled with ϵ by a constant factor. The result suggests $b \simeq 0.5$, a value that we will adopt in the parameterization and the one-column simulations in the next section.

Finally, we initialize the updraft model by taking the mean value at the lowest model level z_1 and adding an excess that scales with the surface flux (Troen and Mahrt 1986)

$$\theta_u(z_1) = \overline{\theta}(z_1) + \alpha \frac{Q_*}{\sigma_w(z_1)}, \tag{17}$$

where $\overline{w'\theta'_s}$ is the surface flux. For the standard deviation σ_w we use the empirical expression (7). The value of the prefactor α again is based on LES results that suggest $\alpha \simeq 1$. Note that this value is much smaller than the value of $\alpha \simeq 8$ originally proposed in (Troen and Mahrt 1986).

This completes the updraft model that calculates, given the surface fluxes and the mean profiles, the updraft fields of θ_u, q_u, and w_u, and the inversion height z_*, the latter being the height where w_u vanishes.

b. Eddy diffusivity and mass flux parameterization

To complete the EDMF approach (5) we need to specify the eddy diffusivity K and the mass flux M. A simple and robust method for the convective boundary layer is to use a profile method (Troen and Mahrt 1986) and we will do so accordingly. A so-called K profile should at least

- obey surface layer similarity near $z = 0$,
- vanish near the inversion,
- exhibit a peak value $K_{\max}/(w_* z_*) \simeq 0.1$.

Holtslag (1998) proposed a K-profile K_h for heat and moisture that obeys these constraints that we will adopt here. In a nondimensionalized form it reads

$$\hat{K}_h \equiv \frac{K_h}{z_* w_*} = k \frac{u_*}{w_*} \phi_{h0}^{-1} \frac{z}{z_*} \left(1 - \frac{z}{z_*}\right)^2, \tag{18}$$

with k the von Kármán's constant and ϕ_{h0} an effective stability function given by

$$\phi_{h0} = \left(1 - 39 \frac{z}{L}\right)^{-1/3}, \tag{19}$$

where L is the Obukhov length. Eliminating the Obukhov length in terms of z_* and w_* finally gives

$$\hat{K}_h = k \left[\left(\frac{u_*}{w_*}\right)^3 + 39k \frac{z}{z_*} \right]^{1/3} \frac{z}{z_*} \left(1 - \frac{z}{z_*}\right)^2. \tag{20}$$

Note that (20) is about proportional to the product of σ_w as given by (7) and a length scale similar to the one given by (16). This observation illustrates the analogy between the present K-profile method and methods in which the eddy-diffusivity is estimated as a product of a length scale and a velocity scale. Since surface layer similarity determines the surface fluxes and the updraft model determines the inversion height z_*, (20) completely determines the eddy diffusivity profile.

The mass-flux $M \simeq a_u w_u$ is directly proportional to w_u since a_u is constant by definition. This allows the mass flux to scale with the standard deviation σ_w (see Fig. 4b)

$$M = c_m \sigma_w, \tag{21}$$

with $c_m \simeq 0.3$ and where we use the parameterized form (7) for σ_w. Alternatively one can also directly use the definition of the mass flux $M \simeq a_u w_u$ and use the updraft velocity equation (15) (Soares et al. 2004).

c. Implementation of the scheme

An often-undervalued aspect of any parameterization is its numerical implementation. The numerical challenge of the present scheme is how to discretize the time evolution equation (2) due to turbulent mixing as estimated by the present EDMF approach (5) for $\phi \in \{\theta, q_v\}$

$$\left(\frac{\partial \overline{\phi}}{\partial t}\right)_{\text{mix}} = -\frac{\partial \overline{w'\phi'}}{\partial z} = -\frac{\partial}{\partial z}\left[-K\frac{\partial \overline{\phi}}{\partial z} + M(\phi_u - \overline{\phi})\right]. \tag{22}$$

In order to solve this advection–diffusion equation in a consistent manner, a full advection–diffusion solver is used. The diffusion and the mass-flux coefficients can be quite large when compared with the time step and vertical grid space typically used in climate and NWP models. In fact, these coefficients often exceed the numerical stability limits for both the diffusion and advection explicit schemes. Because of this, the typical turbulent diffusion equation in climate and NWP models is generally solved in an implicit manner (Girard and Delage 1990; Beljaars 1991).

The advective mass-flux transport, however, is usually treated in an explicit manner, although it has been shown that the mass-flux term violates the stability criterion on a regular basis (Jakob and Siebesma 2003). In order to address these stability problems, the mass-flux and diffusion terms in the present scheme are solved simultaneously in an implicit manner according to an algorithm already tested in the European Centre for Medium-Range Weather Forecasts (ECMWF) model (Teixeira and Siebesma 2000). For details on the numerical discretization of (22), we refer to appendix B.

TABLE 2. The values of the constants based on the LES results that are used in the reference SCM run. The third column shows the variation of these parameters to assess the sensitivity of the scheme to these constants in section 5b.

Parameter	Reference value	Sensitivity variation
c_ϵ	0.4	$0.38 \leq c_\epsilon \leq 0.42$
c_m	0.3	$0.24 \leq c_m \leq 0.36$
b	0.5	$0.4 \leq b \leq 0.6$
μ	0.15	$0.12 \leq \mu \leq 0.18$
α	1.0	$0.8 \leq \alpha \leq 1.2$

5. Single-column model results

a. Reference case

We will proceed by using case 1 as described in section 3 to evaluate the EDMF parameterization. Although this case has been used to design the parameterization, it is still a useful test since it answers the question to which extent the mean turbulent transport in three dimensions can be faithfully represented in one dimension. To this purpose a single-column model (SCM) with the above-described EDMF scheme has been developed. For the time stepping the implicit scheme described in appendix B is used. The values of the constants in the reference case are based on the LES results discussed in the previous section and which are summarized in Table 2.

In order to exclude possible errors due to a too-coarse resolution we use in the reference run the same high vertical resolution of 20 m as in the LES model. Additionally we also repeat the same experiment with a coarser resolution to assess to what extend the parameterization is sensitive to the used vertical resolution. This low-resolution run uses the same resolution as in the 60-level operational ECMWF model (Teixeira 1999). For the present simulations, only the lowest thirteen levels are active, which are at about 10, 35, 75, 125, 200, 295, 410, 560, 730, 930, 1165, 1430, 1725, and 2050 m.

The boundary layer growth is critically dependent on the model formulation of the inversion height z_* because of the use of a K-profile method. Therefore care is needed to determine z_* on a discretized grid in order to avoid possible resolution dependencies. Therefore, two modifications to the model formulation are added. First the inversion height z_*, defined as the height at which the vertical velocity vanishes, is determined by finding the zero-crossing of the updraft velocity by interpolation between the highest level with a positive w_u and the subsequent level that has a negative vertical velocity. This allows a smooth growth of the boundary layer height. Second, since near the inversion the entrainment term becomes increasingly important, we propose a modified formulation of the lateral entrainment to reduce the resolution sensitivity

$$\epsilon \simeq c_\epsilon \left[\frac{1}{z + \Delta z} + \frac{1}{(z_* - z) + \Delta z} \right], \tag{23}$$

where Δz represents the vertical grid size where ϵ is evaluated. Note that in the limit of high-resolution $\Delta z \to 0$ the original formulation (16) is recovered. The addition of the factor Δz assures the entrainment near the inversion can never exceed $c_\epsilon/\Delta z$, which is a reasonable upper limit for the grid-averaged lateral entrainment near the inversion.

Since we do not want that any spinup effects of the LES model runs influence the evaluation, we initialize the SCM with mean profiles of the LES model after 0.5 h of simulation (see Fig. 7a). Figure 7a shows the SCM results after 5 and 10 h of simulation along with the corresponding LES results. It can be observed that the temperature evolution of the boundary layer is well reproduced by the SCM, also in the low-resolution mode. This suggests that the boundary layer growth and the top-entrainment process are well captured by the SCM. This hint is confirmed in Fig. 7b where the boundary layer (BL) height evolution of the SCM is shown and compared with the LES results. The wiggled structure of the BL height growth for the low resolution is the only remnant of the coarse resolution.

Figure 7c focuses more on the internal dynamics of the model. Figure 7c evaluates the nondimensionalized updraft velocity after 10 h of simulation. This result indicates that the updraft model is not only producing the correct boundary layer growth but also the proper updraft characteristics. Finally, in Fig. 7d, the nondimensionalized resulting heat flux after 10 h of simulation is displayed along with the flux from the LES model. Moreover, the breakdown of the turbulent flux of the EDMF scheme into the contribution of the diffusion term and the nonlocal mass flux is shown in the same figure. A couple of remarks should be made here. First it should be observed that both terms contribute to the negative entrainment flux in the inversion: the diffusion term because it is downgradient and the mass-flux contribution because the updraft temperature is lower than the mean temperature in the inversion. Second, the mass-flux term provides, except in the surface layer, the dominant contribution to the turbulent flux. In fact it turns out, as we will see in the next subsection, that the precise magnitude of the eddy diffusivity is not that relevant.

b. Model sensitivity

It is good practice to provide insight on the sensitivity of the parameterization scheme to the used parameters.

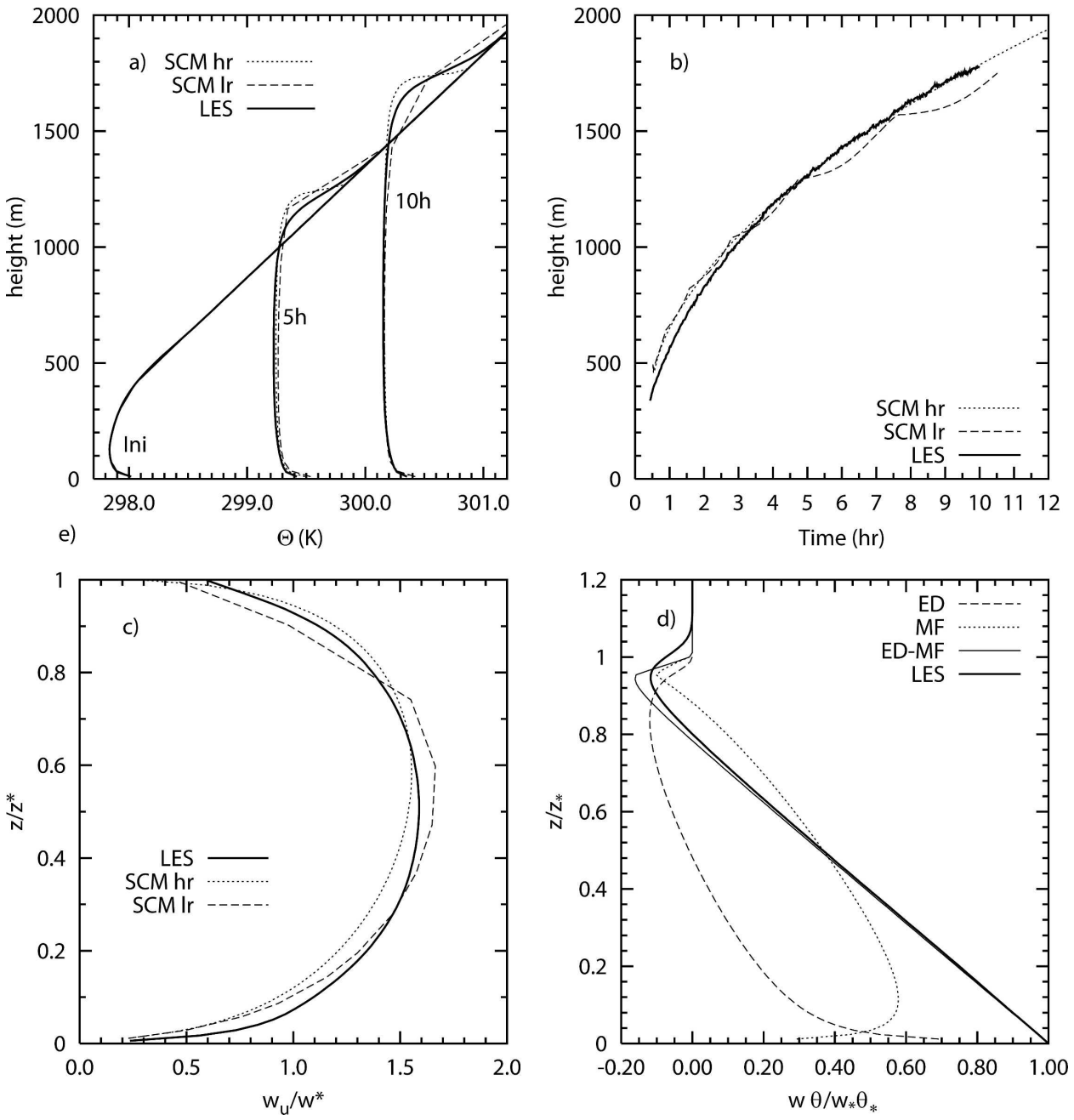

FIG. 7. Single-column model results with a high (dots) and a low (dashes) vertical resolution of the EDMF scheme evaluated with LES results (full lines); (a) initial vertical profile and profiles after 5 and 10 h of simulation, (b) time evolution of the boundary layer height, (c) nondimensionalized updraft velocity of the thermal after 10 h of simulation, and (d) the total nondimensionalized turbulent flux, produced by the LES model (thick full line) and the SCM (thin full line) after 10 h of simulation. Also displayed is the breakdown of the turbulent flux of the EDMF scheme into the diffusion contribution (dashes) and a contribution due to the mass-flux term (dots).

As an integral measure for the sensitivity, the boundary layer height after 10 h of simulation is evaluated. Each of the parameters displayed in Table 2 is increased and decreased by 20% and the effect of this change on the boundary layer height is shown in Fig. 8.

The largest sensitivities are due to the parameters c_ϵ and b, which determine the intensity of the lateral entrainment. The sensitivity c_m that determines the strength of the mass-flux contribution is rather small. Also, the sensitivity to the initialization of the tempera-

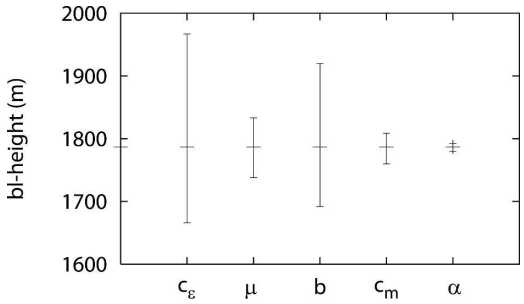

FIG. 8. Effect of the variation of the used constants in the EDMF scheme as given in Table 2 on the boundary layer height after 10 h of simulation. Note that the parameters with the strongest sensitivity are those that directly influence the determination of the BL height.

ture excess as expressed by the factor α is small. This is because the sensitivity is strongly damped by the lateral entrainment of the updraft. In short, the most sensitive parameters are those that directly influence the determination of the boundary layer height, since z_* determines the growth rate of the boundary layer height and hence the top-entrainment flux.

There is also a remarkable insensitivity to the eddy diffusivity K that was already briefly mentioned in the previous subsection. In order to quantify this aspect, the intensity of the K profile (20) is also increased and decreased by 20% without any effect on the model output. In fact, we are able to reduce the effect of the K profile by 80% without any significant effect on the model. Similar to Fig. 7d we show in Fig. 9 the breakup of the total heat flux into the diffusive contribution and the mass-flux contribution after 10 h of simulation for this reduced diffusion case. It can be observed that almost the entire heat flux is faithfully reproduced by the mass-flux contribution only, except near the surface where the diffusion is still the dominant term. One might argue that this observation would promote a parameterization in terms of mass flux only. However, we strongly think that the inclusion of a diffusion term is crucial for a number of reasons. First, in the present convective case it is true that the precise value of the diffusion is not that important, but if we lower the amplitude of the K profile even further by 90% the model becomes unstable near the surface and strong wiggles in the separate flux contributions can be seen. In the present convective case, the diffusion acts mainly as a stabilizing smoothing operator. Second, the role of the diffusion will become more physically relevant in the case of a transition to neutral or stable boundary layer. In that case, the nonlocal mass flux contribution will vanish and the diffusion has to be the main mixing mechanism. With only a mass-flux parameterization, a smooth transition to and a proper parameterization of the neutral and stable boundary layer will become unnecessarily painful.

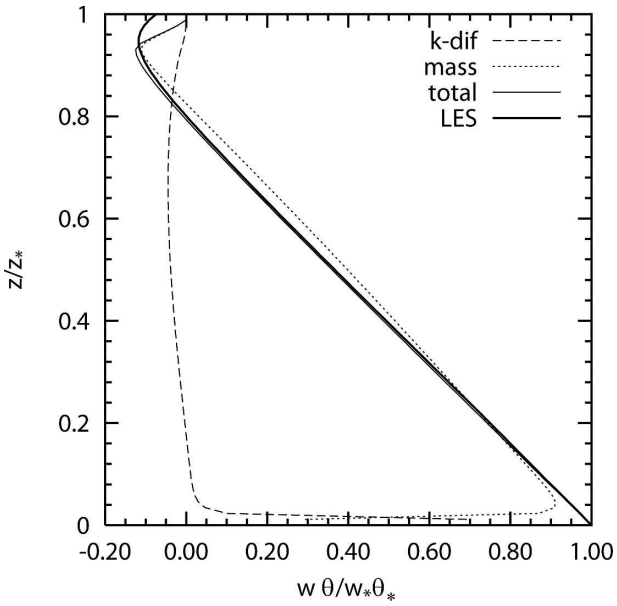

FIG. 9. The same as in Fig. 7d but now with a run in which the K coefficient is reduced by 80% with respect to the reference run. Note that the turbulent flux is almost completely determined by the mass-flux term and that even after 10 h of simulation the SCM flux profile is similar to the flux profile produced by the LES model.

c. *Other approaches*

In this section, we want to confront the EDMF approach with two other more traditional methods. The first one is the usual ED approach without any extra nonlocal modifications. The second approach is to use a countergradient (EDCG) term to take into account nonlocal transport. In formula this second approach is given by (1) where we choose for the nonlocal term γ the formulation suggested by Cuijpers and Holtslag (1998)

$$\gamma = a \frac{w_*}{\sigma_w^2 z_*} \overline{w'\theta'_*}, \tag{24}$$

with $a \simeq 2$. The three approaches are summarized in Table 3. We emphasize that, in order to make the comparison as clean as possible, in all three cases the same K-profile method with the same vertical velocity equation (15) is used to determine the BL height z_*. This way we can assess in a transparent way the impacts of the classic countergradient approach and the mass-flux contribution to the bare eddy diffusivity approach.

TABLE 3. List of the three different approaches to parameterize turbulent transport in the convective boundary layer.

Name	Diffusion	Nonlocal transport
ED	K profile (18)	None
EDMF	K profile (18)	$M(\phi_u - \overline{\phi})$
EDCG	K profile (18)	$K\gamma$

Again as an integral measure, we first show in Fig. 10a the boundary layer growth of all three models for case 1. The results might appear to be somewhat surprising at first sight; the ED model overestimates the boundary layer height indicating too-aggressive boundary layer growth while the EDCG model strongly underestimates this boundary layer growth. In order to explain these results we display the average profiles of θ after 10 h of simulation of the three models along with the LES profile in Fig. 10b. Obviously, since the ED model is apparently too aggressive, the mean temperature in the boundary layer is too high while, on the opposite, the EDCG model underestimates the mean temperature in the boundary layer. Figure 10b also shows that the ED model produces an unrealistic unstable temperature profile. Historically, it is for this reason that the countergradient term has been introduced and indeed, as can be observed in Fig. 10b, the EDCG model gives a stable potential temperature profile in the upper half of the boundary layer. These shapes explain the fact that the ED schemes is more aggressive than the EDCG and the EDMF approach: because of the unrealistic unstable θ profile of the ED approach, the vertical velocity is fed with a too-strong buoyancy source term and, as a result, the updraft penetrates too deep into the inversion. This causes a too-strong entrainment and hence an overaggressive growth of the boundary layer height.

This still leaves the riddle of why the countergradient (EDCG) method is less active than the proposed EDMF method. The reason for this can be easily understood if we again make a breakdown of (1) into the ED contribution and the CG contribution with the format (24) for the 10th hour of the EDCG run (see Fig. 11). Because the countergradient term is always positive, also in the entrainment zone, it reduces the top-entrainment flux. In fact, for the present case the eddy diffusivity and the countergradient term almost balance, so, effectively there is barely any top-entrainment left. Therefore, in short, including a countergradient term has a profound effect of reducing the top-entrainment rate. This explains the slow growth of the BL height of the countergradient experiment when compared with the EDMF approach.

This result might sound somewhat contradictory with respect to previous claims that the nonlocal schemes with a countergradient formulation enhance turbulent mixing leading to deeper boundary layers than with a local scheme without such a countergradient term (Holtslag and Boville 1993; Holtslag et al. 1995). The

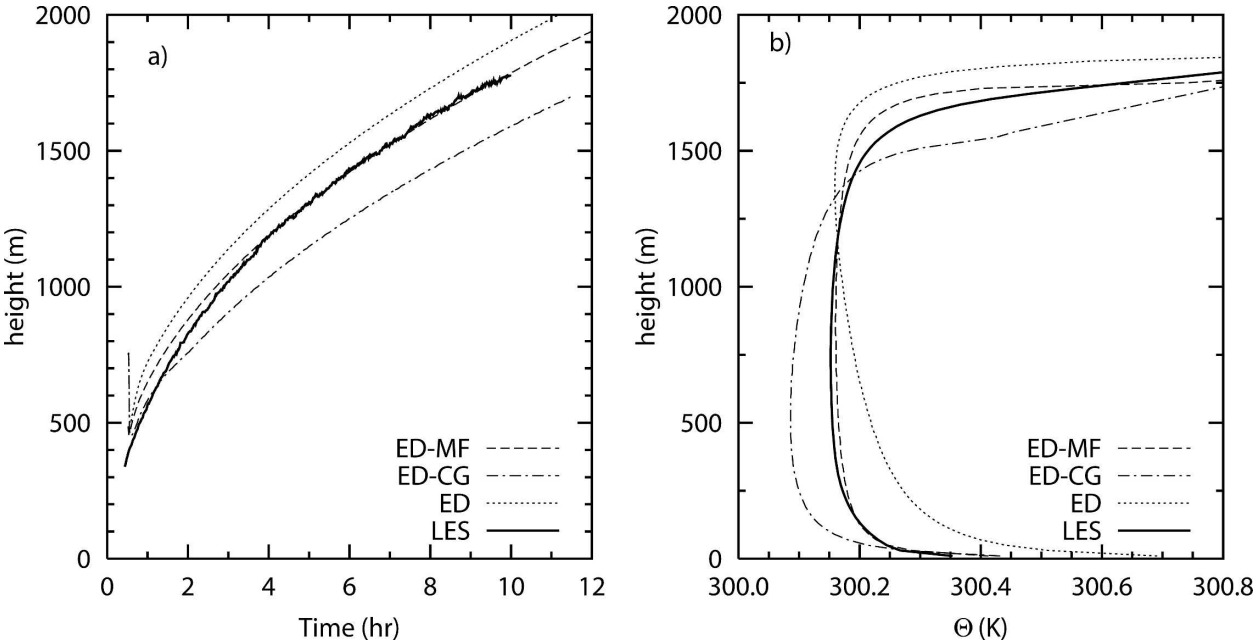

FIG. 10. (a) Time evolution of the inversion height for the three different approaches listed in Table 3 along with LES results as a reference. (b) The mean potential temperature profiles after 10 h of simulation.

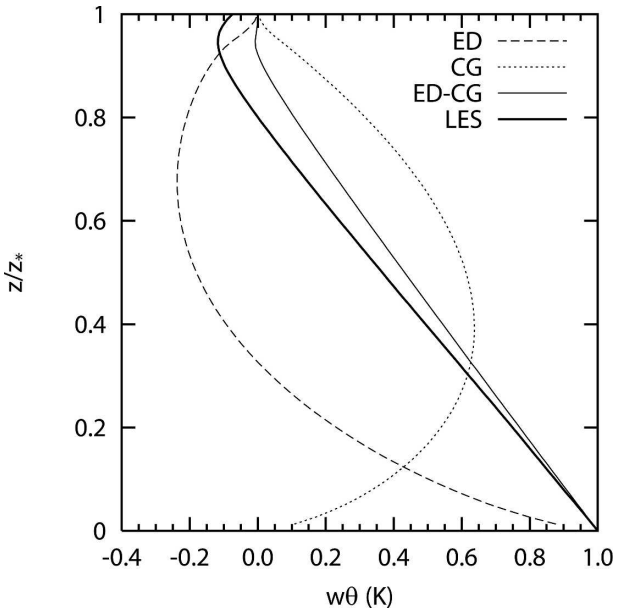

FIG. 11. Total heat flux of the LES model after 10 h of simulation along with the heat flux of the SCM model with the countergradient approach. Also shown is the breakup of the heat flux in the SCM model into a contribution due to the eddy diffusivity and a contribution due to the countergradient term γ. Note that the countergradient contribution is working against the entrainment flux. As a result, there is an almost zero entrainment flux left.

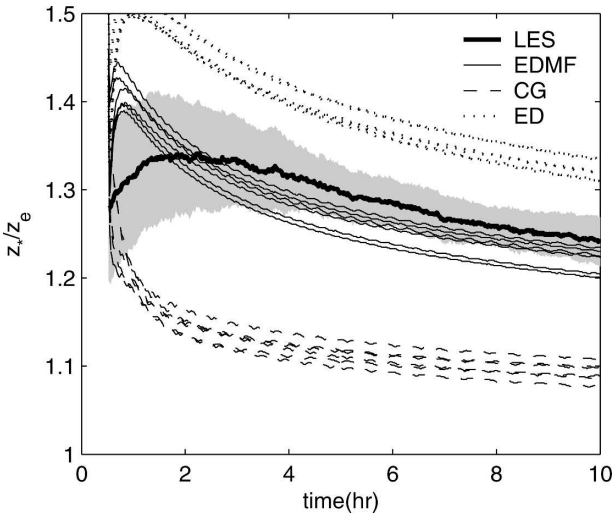

FIG. 12. Dimensionless boundary layer–growth evaluation of the EDMF model (thin full lines), the EDCG model (dashed), and the ED model (dotted) for all six cases defined in Table 1 along with the LES results. These are shown as an ensemble mean (thick line) and a band that indicates the standard deviation of the ensemble.

reason for this is that in these studies, the eddy-diffusivity formulations used for the local and nonlocal schemes are not the same. The reason that the nonlocal scheme appears to be more active despite the countergradient term is due to the use of an aggressive *K*-profile method with a parcel method to estimate the BL height. The present results in this study are qualitatively in agreement with the findings of Stevens (2000) who found, using 1-yr integrations of the standard Community Climate Model (CCM) version 3.2 with fixed SSTs (Kiehl et al. 1996), that switching off the countergradient term leads to an increase of the globally averaged BL height.

d. Evaluation of the model with the other LES cases

So far we have limited our evaluation of the EDMF model and other approaches to case 1. We conclude our study by evaluating the boundary layer growth for all six cases for the reference EDMF model, the EDCG model, and the ED model, and compare these results with the LES data. As already mentioned in section 3, a critical test for these models is whether they can reproduce the dimensionless boundary layer height z_*/z_e for the limit $\hat{t} \to \infty$. As none of these schemes have the level of sophistication to incorporate the dependency of the entrainment flux on the Richardson number (see Fig. 3b), it is not realistic to expect that these 1d-models can reproduce the variation of z_*/z_e from case to case.

The test will therefore be whether the abovementioned models are capable of reproducing values of z_*/z_e that fall within the range of z_*/z_e produced by large-eddy simulations. The LES results are shown in Fig. 12. The thick line is the time evolution of z_*/z_e for the ensemble mean LES results, while the standard deviation of z_*/z_e based on the six cases is shown as a gray band around the mean. The results for all six cases for the EDMF, EDCG, and the ED model are plotted in this Fig. 12 as well. This shows that the results found for case 1 are quite generic: the EDMF model generates boundary layer growth for all cases that fall within the range [1.2, 1.3] and compare reasonably well with the LES results. The EDCG model underestimates the boundary layer growth in all cases while the ED model overestimates the boundary layer growth in all cases.

6. Conclusions and perspectives

Convective boundary layers are ubiquitous in the atmosphere and they have a fundamental impact on the physics and dynamics of the climate system. However, due to coarse horizontal resolution, the turbulent and

convective flow within the boundary layer cannot be explicitly resolved by current weather (global or mesoscale) and climate prediction models. Parameterizations of these subgrid fluxes are then necessary in order to achieve some level of realism. In spite of its apparent simplicity, due to the lack of condensation effects, dry convective boundary layers are still a major challenge in weather and climate modeling, in particular the representation of the boundary layer top-entrainment and the countergradient fluxes.

In this paper we propose a unified way of representing the subgrid vertical flux in dry convective boundary layers, by combining the eddy-diffusivity (ED) approach (typically used for the parameterization of dry and stratus/stratocumulus boundary layers in weather and climate prediction models) with the mass-flux (MF) approach (typically used for the parameterization of shallow and deep moist convection).

The EDMF approach is based on the idea that the MF closure is able to represent what we refer to as nonlocal transport due to the strong thermals, while the ED closure is able to represent the more local turbulent transport. In section 2, it is shown that the EDMF closure follows naturally from a decomposition of the subgrid vertical transport into 1) the strong organized updrafts, and 2) the remaining environment.

In section 3, numerical simulations of the dry convective boundary layer were carried out with a large-eddy simulation (LES) model. These simulations were used to establish the EDMF concept in a more solid base and to obtain estimates for the parameters needed, such as the updraft model, ED and MF coefficients.

LES results were also used to evaluate the new EDMF parameterization. When compared to LES, the new closure represents well the evolution of the main properties of the dry convective boundary layer. The overall growth of the boundary layer is reproduced in an accurate way, even when a relatively poor vertical resolution is used. This result means that the EDMF representation of the top-entrainment must be particularly realistic. The well-mixed nature of the potential temperature profile is achieved in a, probably, unprecedented manner. The linear nature of the buoyancy flux profile, quasi-parabolic nature of the updraft vertical velocity, and updraft temperature are also shown to be realistic when compared to LES results.

Some of the current alternatives, in particular the explicit parameterization of the countergradient fluxes, are analyzed in some detail and compared to the EDMF approach. It is shown that the more traditional countergradient closures indeed reproduce a correct internal structure of the boundary layer, but at the expense of strongly underestimating the ventilating top entrainment. The reason for this last point has been shown to be associated with the negative impact that the countergradient term has at the entrainment level.

Historically, to our knowledge, Chatfield and Brost (1987) were the first to apply a mass-flux approach to an updraft–downdraft decomposition and combine this with an eddy-diffusivity approach for the remaining subplumes to study scalar transport in the dry convective boundary layer. The importance of these subplumes for the total turbulent transport was studied in detail for reactive scalars in the convective boundary layer by Petersen et al. (1999). That concept has been further extended in a higher-order closure framework by Lappen and Randall (2001a,b) and has been applied to both dry and moist convection by these authors.

The present EDMF scheme is based on the ideas from Siebesma and Teixeira (2000) and differs from the previous studies most notably in the definition of the updrafts: since the primary motivation for this study was to establish a continuous formulation between dry thermals in the convective boundary layer and the entraining plumes within the cloud layer, a straightforward updraft–downdraft decomposition is not appropriate. It is for this reason that the strong updraft definition presented in section 3 has been used: LES results show that the strongest updrafts at the top of the subcloud layer actually do form the cloudy cores at cloud base. Therefore, the main advantage of this avenue is that it naturally opens the way for a scheme of the cloud-topped boundary layer by allowing the moisture in the strong updraft to condense. No switching of a moist convection scheme is then necessary anymore. In such a case, the updraft model is always active and decides independently whether these updrafts become cloud-core updrafts or not.

The present version of the EDMF scheme for the dry convective boundary layer is part of the ECMWF model since cycle 29.3 that became operational in April 2005. The EDMF framework also has been implemented successfully in the nonhydrostatic mesoscale atmospheric model of the French research community (Meso-NH; Soares et al. 2004). One main difference with the present formulation is that the eddy-diffusivity in Soares et al. (2004) is calculated using a prognostic turbulent kinetic energy (TKE) equation (Cuxart et al. 2000). Let us emphasize here that the specific choice of how to calculate the eddy diffusivity (TKE or K profile) is important, but not essential for the principle of the EDMF framework.

We would like to conclude with some thoughts on how to extend this framework to the cloudy boundary layer. In Soares et al. (2004), the extension of the

EDMF approach to moist convection has been studied. The updraft equations have been extended by allowing for condensation. Above cloud base, a constant fractional entrainment rate of $\epsilon = 2\ 10^{-3}\ \mathrm{m}^{-1}$ is used and the mass flux is determined below cloud base by $M = a_u w_u$ where the updraft velocity w_u follows from the updraft equation (15), while above cloud base the mass flux is simply diagnosed from the cloud-core continuity equation (8). This form of the EDMF scheme has been implemented in the Meso-NH model and evaluated with observations from the Atmospheric Radiation Measurement (ARM) Southern Great Plains (SGP) site on 21 June 1997 during which a typical diurnal cycle of cumulus convection was observed (Brown et al. 2002; Lenderink et al. 2004).

At ECMWF, the EDMF framework has been extended by enhancing the dry K profile (20) to moist conditions in order to allow for diffusive mixing in the stratocumulus-topped boundary layer as proposed by van Meijgaard and van Ulden (1998). The eddy diffusivity is then based on both surface and cloud-top forcing. This parameterization is operational since April 2005 and drastically improves the representation of marine stratocumulus with additional benefits to continental winter stratus (Koehler 2005). At the moment, the EDMF framework is being extended to shallow convection as well in the ECMWF model using multiple mass-flux terms (Cheinet 2003). The EDMF approach has also been recently successfully applied to pollutant transport in the cumulus-topped boundary layer (Angevine 2005).

A number of open questions still remain that provide an active source of research at this moment. First, there is the issue of what to use for the fractional entrainment formulation. Soares et al. (2004) essentially use a combination of the present formulation (16) combined with a typical constant value above cloud base that is diagnosed from LES studies for shallow cumulus convection (Brown et al. 2002; Siebesma et al. 2003). An interesting alternative has been proposed by Cheinet (2003) and is a combination of the present formulation (16) and a formulation that has been proposed in Neggers et al. (2002)

$$\epsilon \equiv \max\left(\frac{1}{\tau w_u}, \frac{c_\epsilon}{z}\right), \tag{25}$$

where τ represents the eddy turnover time. In the lower part of the boundary layer the c_ϵ/z term dominates while in the upper part of the boundary layer and in the cloud layer the entrainment rate is determined by $1/(\tau w_u)$. Indeed the fractional entrainment rate is about inversely proportional to the updraft vertical velocity. The simple rational behind this behavior is that slow updrafts have simply more time to mix with environmental air than fast updrafts. This formulation has the advantage that it works in the cloud layer as well as in the subcloud layer and, moreover, it does not require the inversion height z_* as an input variable. Second, there is the issue of the updraft velocity equation. The formulation (15) is identical to formulations used in moist convection schemes (Gregory 2001) but with different coefficients. A similar diagnosis for the updraft velocity equation in the cloudy core should shed some light on this issue. Third, there is the issue of the mass flux. For the clear boundary layer, one can use the vertical velocity variance to scale the mass-flux (21) but this scaling does not hold anymore in the cloud layer. Using the updraft velocity w_u instead (Soares et al. 2004) is an interesting alternative that automatically provides a closure for the mass flux at cloud base that is closely related to the mass-flux closures proposed by Grant (2001) and Neggers et al. (2004).

Let us finally note that the present proposed formulation can be extended to multiple entraining plumes. Recent studies have shown that multiple entraining plumes can give an accurate description of the turbulent transport and the variability in both the clear (Cheinet 2003) and the cloud-topped boundary layer (Cheinet 2004; Neggers et al. 2002). The present study, however, shows that, as far turbulent transport in the convective dry boundary layer is concerned, one updraft equation is sufficient.

Acknowledgments. This research was initiated while the first author, A. Pier Siebesma, was invited to work as a consultant at the ECMWF. It is therefore a pleasure to thank Anton Beljaars and Martin Miller for their keen interest in this topic. We also want to thank Aad van Ulden for many useful suggestions during earlier stages of the design of this scheme. Bjorn Stevens and two anonymous reviewers are acknowledged for the many valuable suggestions on a first draft of the paper and Stephan de Roode and Geert Lenderink for a critical reading of the manuscript. The work done by Pedro M. M. Soares was supported by Fundacão para a Ciência e Tecnologia (FCT) under Project BOSS/58932/2004, cofinanced by the European Union under Program FEDER, and by the EU Grant EVK2 CT1999 0005 (EUROCS).

APPENDIX A

Analytical Results for the Updraft Fields in the Surface Layer

LES results suggest a power-law behavior of ϵ near the surface

$$\epsilon \simeq \frac{c_\epsilon}{z}. \tag{A1}$$

If we use substitute this in the updraft equation for a field ϕ

$$\frac{\partial \phi_u}{\partial z} = -\epsilon(\phi_u - \overline{\phi}), \tag{A2}$$

we obtain a general solution of the form

$$\phi_u(z) = Az^{-c_\epsilon} + c_\epsilon z^{-c_\epsilon} \int \overline{\phi}(z) z^{c_\epsilon - 1}\, dz. \tag{A3}$$

Assuming a logarithmic profile for $\overline{\phi}$ in the surface layer

$$\overline{\phi}(z) = \overline{\phi}(z_0) - c_\phi \ln \frac{z}{z_0}, \tag{A4}$$

and an excess of $\Delta\phi_u(z_0)$ of the updraft field at an arbitrary height z_0 in the surface layer; that is, $\phi_u(z_0) = \overline{\phi}(z_0) + \Delta\phi_u(z_0)$, we find

$$\phi_u(z) = \overline{\phi}(z_0) + \Delta\phi_u(z_0) - c_\phi \ln \frac{z}{z_0}, \tag{A5}$$

which directly proves that that the excess of the updraft field; that is, $\phi_u(z) - \overline{\phi}(z)$, remains constant as a function of height. This implies that the updraft field $\phi_u(z)$ does not depend on the position z_0 in the surface layer where it is initialized.

APPENDIX B

Discretization of the EDMF Equation

Equation (22) is solved with the following discretization in time

$$\frac{\phi^{t+\Delta t} - \phi^t}{\Delta t} = -\frac{\partial}{\partial z}\left[-K^t \frac{\partial \phi^{t+\Delta t}}{\partial z} + M^t(\phi_u^t - \phi^{t+\Delta t})\right], \tag{B1}$$

where we skipped the average bar in order to simplify notation. The generic variable ϕ on the rhs is taken implicitly, but the ED and MF coefficients and the updraft fields are taken explicitly. This occurs due to the nonlinear way of calculating these coefficients, which would lead to nonlinear implicit solvers if the coefficients were considered in an implicit manner.

For the space discretization, centered differences in space are used for the diffusion term and an upwind scheme is used for the mass-flux term. The fully discretized version of the equation is (assuming K and M are constant in space for notation simplicity)

$$-\alpha\phi_{z-\Delta z}^{t+\Delta t} + (1 + 2\alpha + \beta)\phi_z^{t+\Delta t} - (\alpha + \beta)\alpha\phi_{z+\Delta z}^{t+\Delta t} = \phi_z^t + C_z^t, \tag{B2}$$

where $\alpha = K^t\Delta t/\Delta z^2$ and $\beta = M^t\Delta t/\Delta z$ and the term C contains the source terms and the term that involves the updraft values that are taken explicit in time.

Although the present model has not shown any stability problems with the resolutions and time steps that were used, and since the different prognostic equations can be highly nonlinear, the present quasi-implicit scheme proposed may not be sufficiently stable for all cases. This is actually a common and open problem in weather and climate prediction models and in the future more stable solutions will be necessary.

REFERENCES

Angevine, W. M., 2005: An integrated turbulence scheme for boundary layers with shallow cumulus applied to pollutant transport. *J. Appl. Meteor.,* **44,** 1436–1452.

Arakawa, A., 1969: Parameterization of cumulus convection. *Proc. IV WMO/IUGG Symp. on Numerical Prediction,* Vol. 8, Tokyo, Japan, Japan Meteorological Agency, 1–6.

Beljaars, A. C. M., 1991: Numerical schemes for parameterizations. *Proc. Seminar on Numerical Methods in Atmospheric Models,* Reading, United Kingdom, ECMWF, 1–42.

Betts, A. K., 1973: Non-precipitating cumulus convection and its parameterization. *Quart. J. Roy. Meteor. Soc.,* **99,** 178–196.

Bougeault, P., and P. Lacarrère, 1989: Parameterization of orography-induced turbulence in a mesobeta-scale model. *Mon. Wea. Rev.,* **117,** 1872–1890.

Brown, A. R., and Coauthors, 2002: Large-eddy simulation of the diurnal cycle of shallow cumulus convection over land. *Quart. J. Roy. Meteor. Soc.,* **128,** 1075–1094.

Chatfield, R. B., and R. A. Brost, 1987: A two-stream model of the vertical transport of trace species in the convective boundary layer. *J. Geophys. Res.,* **92,** 13 263–13 276.

Cheinet, S., 2003: A multiple mass-flux parameterization for the surface-generated convection. Part I: Dry plumes. *J. Atmos. Sci.,* **60,** 2313–2327.

——, 2004: A multiple mass flux parameterization for the surface-generated convection. Part II: Cloudy cores. *J. Atmos. Sci.,* **61,** 1093–1113.

Cuijpers, J. W. M., and P. J. Duynkerke, 1993: Large-eddy simulation of trade-wind cumulus clouds. *J. Atmos. Sci.,* **50,** 3894–3908.

——, and A. A. M. Holtslag, 1998: Impact of skewness and nonlocal effects on scalar and buoyancy fluxes in convective boundary layers. *J. Atmos. Sci.,* **55,** 151–162.

Cuxart, J., P. Bougeault, and J.-L. Redelsperger, 2000: A turbulence scheme allowing for mesoscale and large-eddy simulations. *Quart. J. Roy. Meteor. Soc.,* **126,** 1–30.

Deardorff, J. W., 1966: The counter-gradient heat flux in the lower atmosphere and in the laboratory. *J. Atmos. Sci.,* **23,** 503–506.

——, 1972: Theoretical expression for the counter-gradient vertical heat flux. *J. Geophys. Res.,* **77,** 5900–5904.

de Haij, M. J., 2005: Evaluation of a new trigger function of convection. KNMI Tech. Rep. TR-276, 117 pp.

de Roode, S. R., and C. S. Bretherton, 2003: Mass-flux budgets of shallow cumulus clouds. *J. Atmos. Sci.,* **60,** 137–151.

——, P. G. Duynkerke, and A. P. Siebesma, 2000: Analogies between mass-flux and Reynolds-averaged equations. *J. Atmos. Sci.,* **57,** 1585–1598.

Ertel, H., 1942: Der vertikale Turbulenz-Wärmestrom in der Atmosphäre. *Meteor. Z.,* **59,** 1690–1698.

Fedorovich, E., R. Conzemius, and D. Mironov, 2004: Convective entrainment into a shear-free, linearly stratified atmosphere: Bulk models reevaluated through large eddy simulations. *J. Atmos. Sci.,* **61,** 281–295.

Girard, C., and Y. Delage, 1990: Stable schemes for nonlinear vertical diffusion in atmospheric circulation models. *Mon. Wea. Rev.,* **118,** 737–746.

Grant, A. L. M., 2001: Cloud-base fluxes in the cumulus-capped boundary layer. *Quart. J. Roy. Meteor. Soc.,* **127,** 407–422.

Gregory, D., 2001: Estimation of entrainment rate in simple models of convective clouds. *Quart. J. Roy. Meteor. Soc.,* **127,** 53–72.

Holtslag, A. A. M., 1998: Modelling of atmospheric boundary layers. *Clear and Cloudy Boundary Layers,* A. A. M. Holtslag and P. G. Duynkerke, Eds., North Holland Publishers, 85–110.

——, and C.-H. Moeng, 1991: Eddy diffusivity and countergradient transport in the convective atmospheric boundary layer. *J. Atmos. Sci.,* **48,** 1690–1698.

——, and B. A. Boville, 1993: Local versus nonlocal boundary-layer diffusion in a global climate model. *J. Climate,* **6,** 1825–1842.

——, E. van Meijgaard, and W. C. de Rooy, 1995: A comparison of boundary layer diffusion schemes in unstable conditions over land. *Bound.-Layer Meteor.,* **76,** 69–95.

Jakob, C., and A. P. Siebesma, 2003: A new subcloud model for mass-flux convection schemes: Influence on triggering, updraft properties, and model climate. *Mon. Wea. Rev.,* **131,** 2765–2778.

Kiehl, J. T., J. J. Hack, G. B. Bonan, B. Boville, B. P. Briegleb, D. L. Williamson, and P. J. Rasch, 1996: Description of the NCAR Community Climate Model (CCM3). NCAR Tech. Rep. 420, 152 pp.

Koehler, M., 2005: Improved prediction of boundary layer clouds. *ECMWF Newsletter,* No. 104, ECMWF, Reading, United Kingdom, 18–22.

Krusche, N., and A. P. Oliveira, 2004: Characterization of coherent structures in the atmospheric surface layer. *Bound.-Layer Meteor.,* **110,** 191–211.

Lappen, C.-L., and D. A. Randall, 2001a: Toward a unified parameterization of the boundary layer and moist convection. Part I: A new type of mass-flux model. *J. Atmos. Sci.,* **58,** 2021–2036.

——, and ——, 2001b: Toward a unified parameterization of the boundary layer and moist convection. Part II: Lateral mass exchanges and subplume-scale fluxes. *J. Atmos. Sci.,* **58,** 2037–2051.

Lemone, M. A., and W. T. Pennell, 1976: The relationship of trade wind cumulus distribution to subcloud layer fluxes and structure. *Mon. Wea. Rev.,* **104,** 524–539.

Lenderink, G., and Coauthors, 2004: The diurnal cycle of shallow cumulus clouds over land: A single-column model intercomparison study. *Quart. J. Roy. Meteor. Soc.,* **130,** 3339–3364.

Lenschow, D. H., and P. L. Stephens, 1980: The role of thermals in the convective boundary layer. *Bound.-Layer Meteor.,* **19,** 509–532.

Neggers, R. A. J., A. P. Siebesma, and H. J. J. Jonker, 2002: A multiparcel model for shallow cumulus convection. *J. Atmos. Sci.,* **59,** 1655–1668.

——, ——, G. Lenderink, and A. A. M. Holtslag, 2004: An evaluation of mass flux closures for diurnal cycles of shallow cumulus. *Mon. Wea. Rev.,* **132,** 2525–2538.

Nieuwstadt, F. T. M., P. J. Mason, C.-H. Moeng, and U. Schumann, 1991: Large-eddy simulation of the convective boundary layer: A comparison of four computer codes. *Turbulent Shear Flows 8,* F. Durst et al., Eds., Springer-Verlag, 343–367.

Ogura, Y., and H.-R. Cho, 1973: Diagnostic determination of cumulus cloud populations from observed large-scale variables. *J. Atmos. Sci.,* **30,** 1276–1286.

Petersen, A. C., C. Beets, H. van Dop, P. G. Duynkerke, and A. P. Siebesma, 1999: Mass-flux characteristics of reactive scalars in the convective boundary layer. *J. Atmos. Sci.,* **56,** 37–56.

Randall, D. A., Q. Shao, and C.-H. Moeng, 1992: A second-order bulk boundary-layer model. *J. Atmos. Sci.,* **49,** 1903–1923.

Schumann, U., and C.-H. Moeng, 1991: Plume budgets in clear and cloudy convective boundary layers. *J. Atmos. Sci.,* **48,** 1758–1770.

Siebesma, A. P., and J. W. M. Cuijpers, 1995: Evaluation of parametric assumptions for shallow cumulus convection. *J. Atmos. Sci.,* **52,** 650–666.

——, and A. A. M. Holtslag, 1996: Model impacts of entrainment and detrainment rates in shallow cumulus convection. *J. Atmos. Sci.,* **53,** 2354–2364.

——, and J. Teixeira, 2000: An advection-diffusion scheme for the convective boundary layer: Description and 1d-results. *Proc. 14th Symp. on Boundary Layers and Turbulence,* Aspen, CO, Amer. Meteor. Soc., 133–136.

——, and Coauthors, 2003: A large eddy simulation intercomparison study of shallow cumulus convection. *J. Atmos. Sci.,* **60,** 1201–1219.

Simpson, J., and V. Wiggert, 1969: Models of precipitating cumulus towers. *Mon. Wea. Rev.,* **97,** 471–489.

Soares, P. M. M., P. M. A. Miranda, A. P. Siebesma, and J. Teixeira, 2004: An eddy-diffusivity/mass-flux parameterization for dry and shallow cumulus convection. *Quart. J. Roy. Meteor. Soc.,* **130,** 3365–3384.

Stevens, B., 2000: Quasi-steady analysis of a PBL model with an eddy-diffusivity profile and nonlocal fluxes. *Mon. Wea. Rev.,* **128,** 824–836.

——, and Coauthors, 2001: Simulations of trade wind cumuli under a strong inversion. *J. Atmos. Sci.,* **58,** 1870–1891.

Stull, R. B., 1988: *An Introduction to Boundary Layer Meteorology.* Kluwer Academic, 666 pp.

Sullivan, P. P., C.-H. Moeng, B. Stevens, D. H. Lenschow, and S. D. Mayor, 1998: Structure of the entrainment zone capping the convective atmospheric boundary layer. *J. Atmos. Sci.,* **55,** 3042–3064.

Teixeira, J., 1999: The impact of increased boundary layer vertical resolution on the ECMWF forecast system. ECMWF Tech. Rep. 268, 55 pp.

——, and A. P. Siebesma, 2000: A mass-flux/K-diffusion approach to the parameterization of the convective boundary layer: Global model results. *Proc. 14th Symp. on Boundary Layers and Turbulence,* Aspen, CO, Amer. Meteor. Soc., 231–234.

——, J. P. Ferreira, P. M. A. Miranda, T. Haack, J. Doyle, A. P. Siebesma, and R. Salgado, 2004: A new mixing-length formulation for the parameterization of dry convection: Implementation and evaluation in a mesoscale model. *Mon. Wea. Rev.,* **132,** 2698–2707.

Tiedtke, M., W. A. Hackley, and J. Slingo, 1988: Tropical forecasting at ECMWF: The influence of physical parameterization on the mean structure of forecasts and analyses. *Quart. J. Roy. Meteor. Soc.,* **114,** 639–664.

Troen, I., and L. Mahrt, 1986: A simple model of the atmospheric boundary layer: Sensitivity to surface evaporation. *Bound.-Layer Meteor.,* **37,** 129–148.

van Meijgaard, E., and A. P. van Ulden, 1998: A first order mixing-condensation scheme for nocturnal stratocumulus. *Atmos. Res.,* **45,** 253–273.

van Ulden, A. P., and A. P. Siebesma, 1997: A model for strong updrafts in the convective boundary layer. Preprints, *12th Symp. on Boundary Layers and Turbulence,* Vancouver, BC, Canada, Amer. Meteor. Soc, 257–259.

Wang, S., and B. A. Albrecht, 1990: A mean-gradient model of the dry convective boundary layer. *J. Atmos. Sci.,* **47,** 126–138.

Wyngaard, J. C., and C.-H. Moeng, 1992: Parameterizing turbulent diffusion through the joint probability density. *Bound.-Layer Meteor.,* **60,** 1–13.

Yanai, M., S. Esbensen, and J.-H. Chu, 1973: Determination of bulk properties of tropical cloud clusters from large-scale heat and moisture budgets. *J. Atmos. Sci.,* **30,** 611–627.